Heterometallic 3d-4f single molecule magnets: Ligand and metal ion influences on the magnetic relaxation

Stuart K. Langley,[§] Crystal Le, [§]Liviu Ungur, [‖] Boujemaa Moubaraki, [§] Brendan F. Abrahams,[†] Liviu F. Chibotaru*[‖] and Keith S. Murray*[§]

TOC synopsis

The structures, magnetism and ab initio calculations for a range of $\{M(III)_2Dy(III)_2\}$-alcoholamine butterfly-shaped clusters (M = Co, Cr), containing a variety of substituted carboxylate and β-diketonate co-ligands, reveal new insights into the factors that influence barrier heights, relaxation rates and hysteresis. As well as the geometry around the Dy centers, factors such as electron withdrawing properties on co-ligand substituents influence the relaxation. Exchange coupling, particularly in the Cr derivatives, reveal a multilevel exchange relaxation mechanism.

Supporting Information

Heterometallic 3d-4f single molecule magnets: Ligand and metal ion influences on the relaxation

Stuart K. Langley, Crystal Le, Liviu Ungur, Boujemaa Moubaraki, Brendan F. Abrahams, Liviu F. Chibotaru* and Keith S. Murray*

Table S1. Crystallographic data for complexes **1** – **6**.

	1	**2**	**3**	**3a**	**4**
Formula[A]	$Co_2Dy_2C_{46}H_{56}O_{20}N_4Cl_4$	$Co_2Dy_2C_{66}H_{110}O_{25}N_4$	$Co_3DyC_{32}H_{61}O_{20}N_6$	$Co_3GdC_{32}H_{61}O_{20}N_6$	$Co_2Dy_2C_{50}H_{58}O_{21}N_4F_{12}$
M, $gmol^{-1}$	1569.61	1802.42	1189.16	1183.91	1721.86
Crystal system	Triclinic	Monoclinic	Monoclinic	Monoclinic	Triclinic
Space group	*P-1*	*$P2_1/n$*	*$P2_1/c$*	*$P2_1/c$*	*P-1*
a/[Å]	10.417(2)	15.3861(5)	15.0304(5)	15.6274(9)	8.9740(3)
b/[Å]	11.400(2)	18.3090(6)	14.3735(5)	14.5047(7)	11.5586(4)
c/[Å]	11.740(2)	28.4364(9)	24.1136(8)	24.1348(11)	15.6439(5)
α/[°]	73.14(3)	90	90	90	81.454(2)
β/[°]	89.79(3)	104.4810(10)	101.168(2)	102.803(5)	77.599(3)
γ/[°]	81.32(3)	90	90	90	72.244(3)
V/[$Å^3$]	1317.8(5)	7756.2(4)	5110.8(3)	5334.6(5)	1503.30(9)
T/K	100(2)	123(2)	100(2)	173(2)	123(2)
Z	1	4	4	4	1
$\rho_{,calc}$ [g cm^{-3}]	1.978	1.542	1.545	1.474	1.901
Λ^B/ [Å]	0.71079	0.71073	0.71073	0.71073	0.71073
Data Measured	15842	38194	60475	43391	13883
Ind. Reflns	4232	22530	15351	12188	6898
R_{int}	0.0781	0.0321	0.0334	0.0685	0.0357
Reflns with I > 2σ(I)	4159	15574	11490	8761	6170
Parameters	354	920	570	574	429
Restraints	0	3	15	55	0
R_1^C(obs), wR_2^C (all)	0.0386, 0.0970	0.0466,0.1111	0.0540, 0.1773	0.0610, 0.2008	0.0281, 0.0588
goodness of fit	1.031	1.021	1.070	1.078	1.060
Largest residuals/[e Å $^{-3}$]	0.877, -1.011	1.802,-1.505	2.615, -2.293	1.538, -1.101	1.117, -0.730

	5	6
Formula[A]	$Co_2Dy_2C_{38}H_{53}O_{18}N_4F_{21}$	$Cr_2Dy_2C_{42}H_{34}O_{18}N_2F_{36}$
M, $gmol^{-1}$	1695.70	1967.71
Crystal system	Triclinic	Orthorhombic
Space group	*P-1*	*Pbca*
a/[Å]	10.9187(5)	17.6229(9)
b/[Å]	16.0291(6)	18.9489(9)
c/[Å]	16.6326(7)	19.4315(10)
α/[°]	78.848(2)	90
β/[°]	79.658(2)	90
γ/[°]	79.944(2)	90
V/[$Å^3$]	2780.0(2)	6488.9(6)
T/K	123(2)	123(2)
Z	2	4
$\rho_{, calc}$ [g cm^{-3}]	2.026	2.014
Λ^B/ [Å]	0.71073	0.71073
Data Measured	43943	33709
Ind. Reflns	12670	9524
R_{int}	0.0230	0.0376
Reflns with I > 2σ(I)	11297	6895
Parameters	834	490
Restraints	72	36
R_1^C(obs), wR_2^C (all)	0.0205, 0.0463	0.0387, 0.0916
goodness of fit	1.036	1.074
Largest residuals/[e Å $^{-3}$]	1.002, -0.755	1.324, -0.923

[A] Including solvate molecules. [B] Graphite monochromator.

[C] $R1 = \Sigma||F_o| - |F_c||/\Sigma|F_o|$, $wR2 = \{\Sigma[w(F_o^2-F_c^2)^2]/\Sigma[w(F_o^2)^2]\}^{1/2}$.

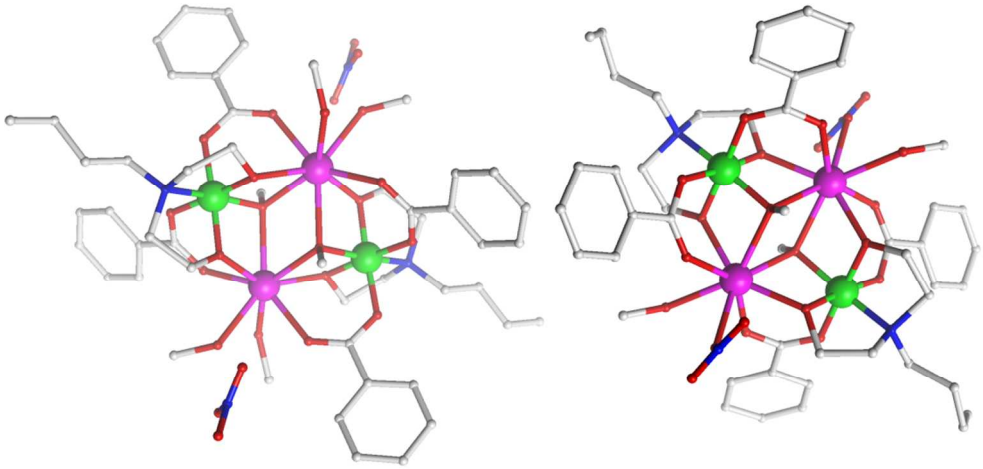

Figure S1. Molecular structure of $[Co^{III}_2Dy^{III}_2(OMe)_2(O_2CPh)_4(bdea)_2(MeOH)_4](NO_3)_2$ (left) and $[Co^{III}_2Dy^{III}_2(OMe)_2(O_2CPh)_4(bdea)_2(NO_3)_2(MeOH)_2]$ (right) which are found in the same crystal. Colour scheme; Co^{III}, green; Dy^{III}, purple; O, red; N, blue; C, grey

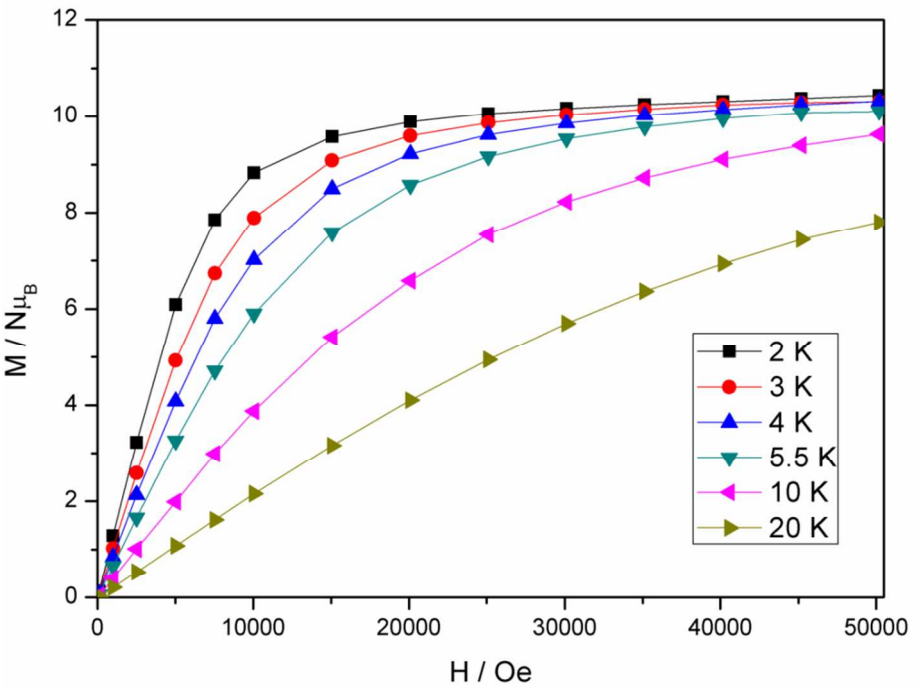

Figure S2. Isothermal magnetization *versus* field plot for **1**.

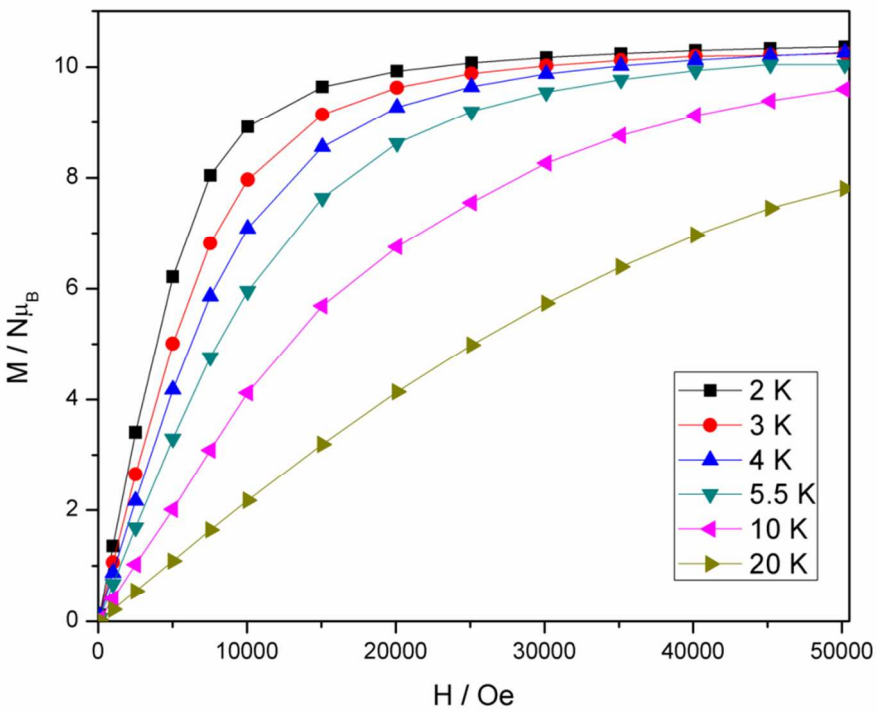

Figure S3. Isothermal magnetization *versus* field plot for **2**.

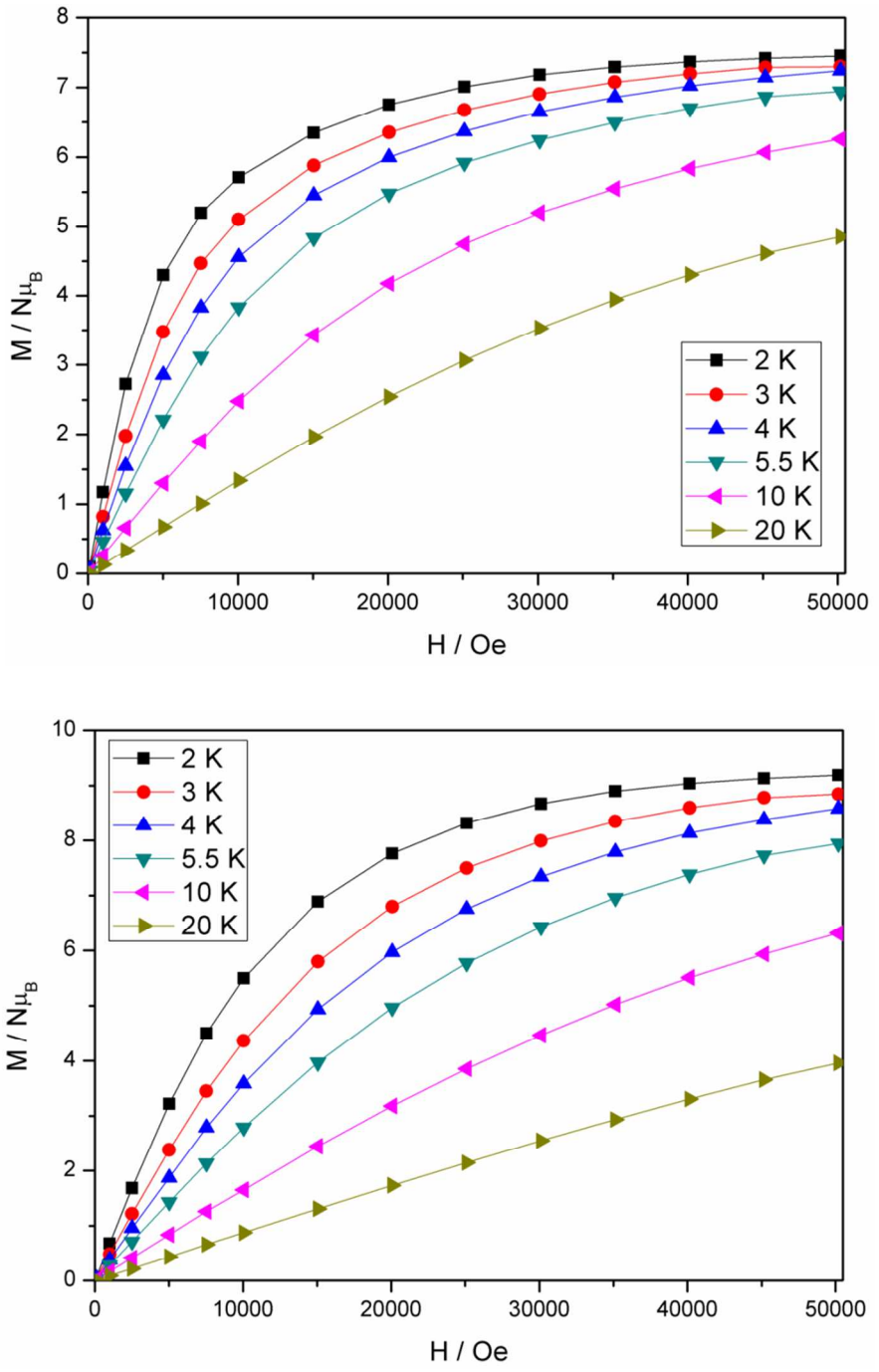

Figure S4. (top) Isothermal magnetization *versus* field plot for **3**; (bottom) Isothermal magnetization *versus* field plot for **3a**.

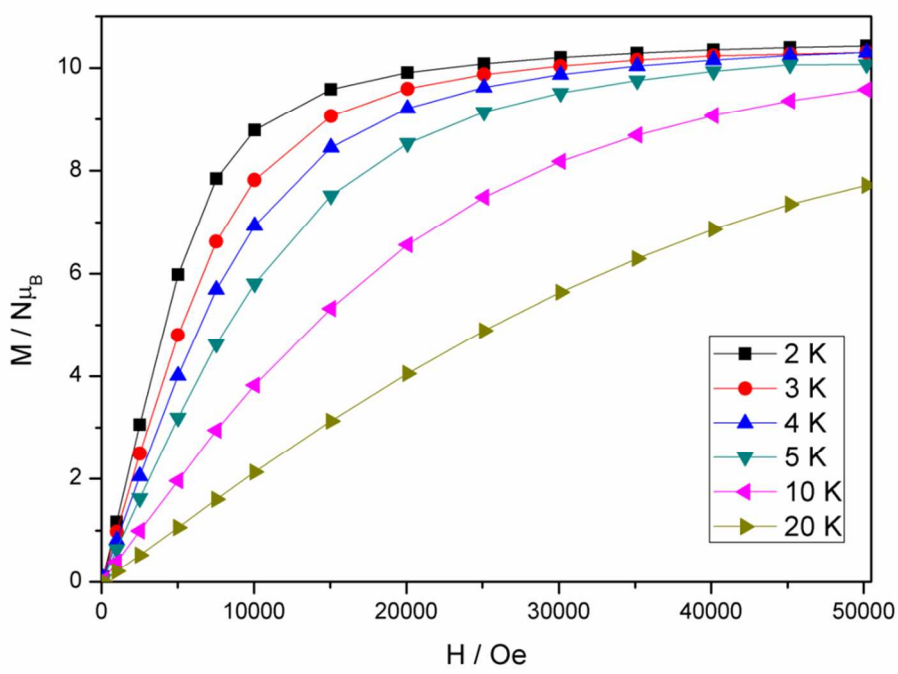

Figure S5. Isothermal magnetization *versus* field plot for **4**.

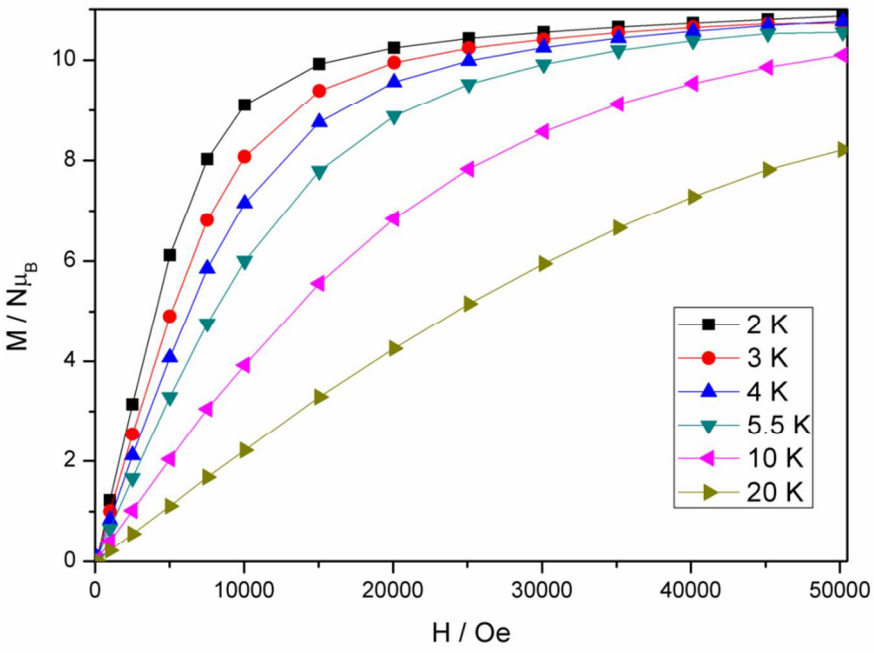

Figure S6. Isothermal magnetization *versus* field plot for **5**.

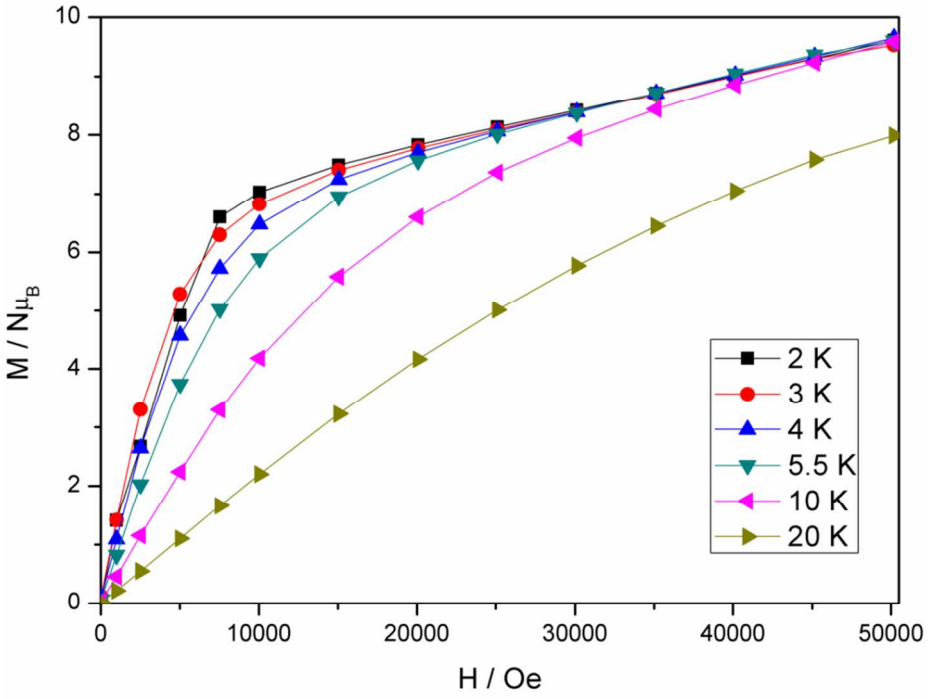

Figure S7. Isothermal magnetization *versus* field plot for **6**.

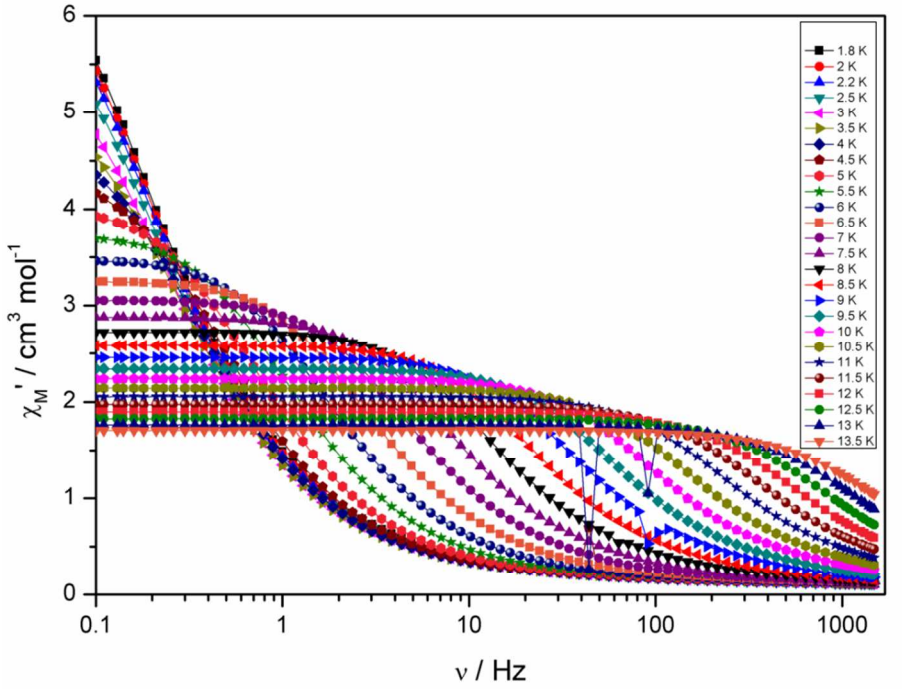

Figure S8. In-phase susceptibility (χ_M') *versus* frequency for **1**.

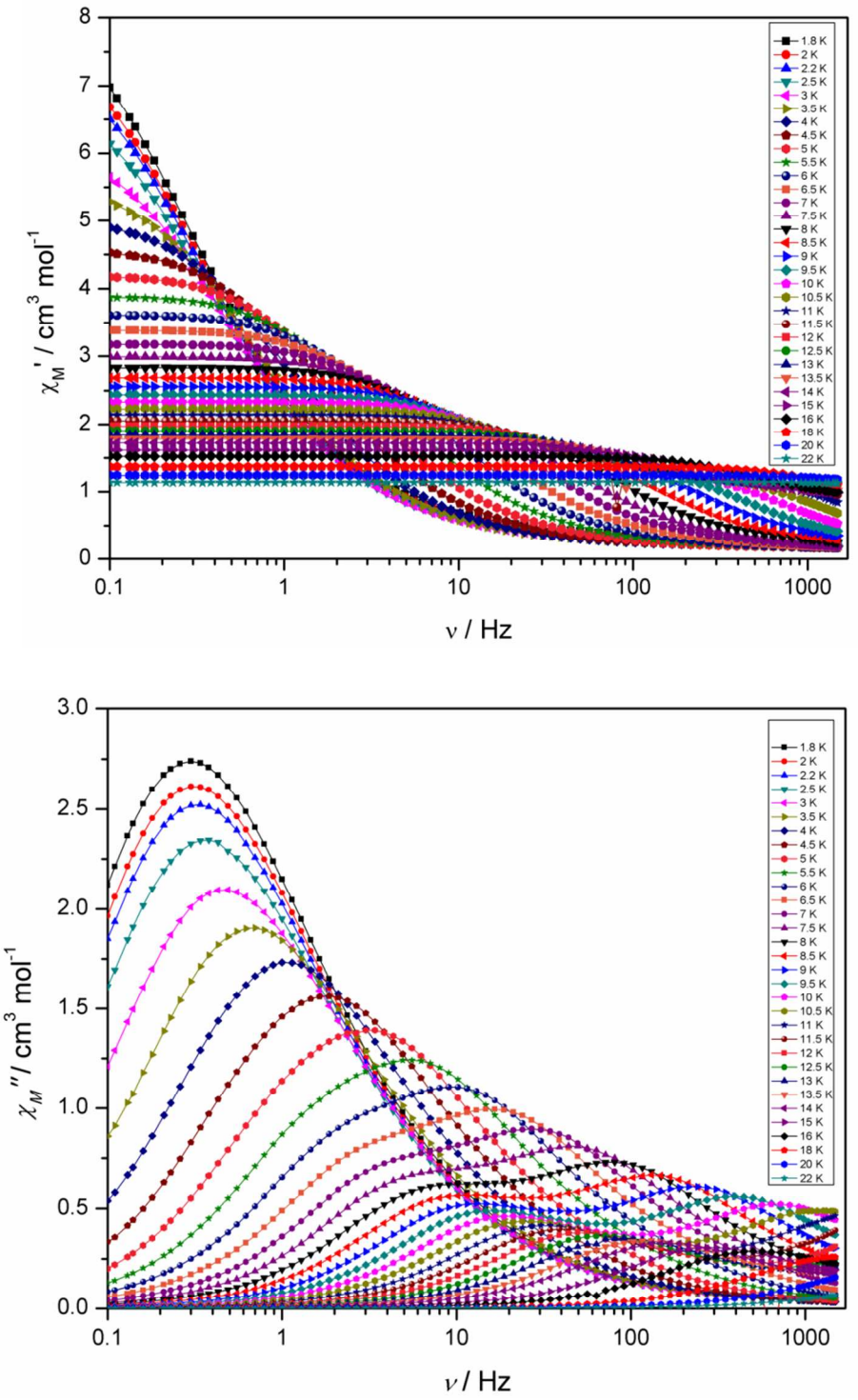

Figure S9. (top) In-phase susceptibility (χ_M') *versus* frequency for **2**; (bottom) Out-of-phase susceptibility (χ_M") versus frequency for **2**.

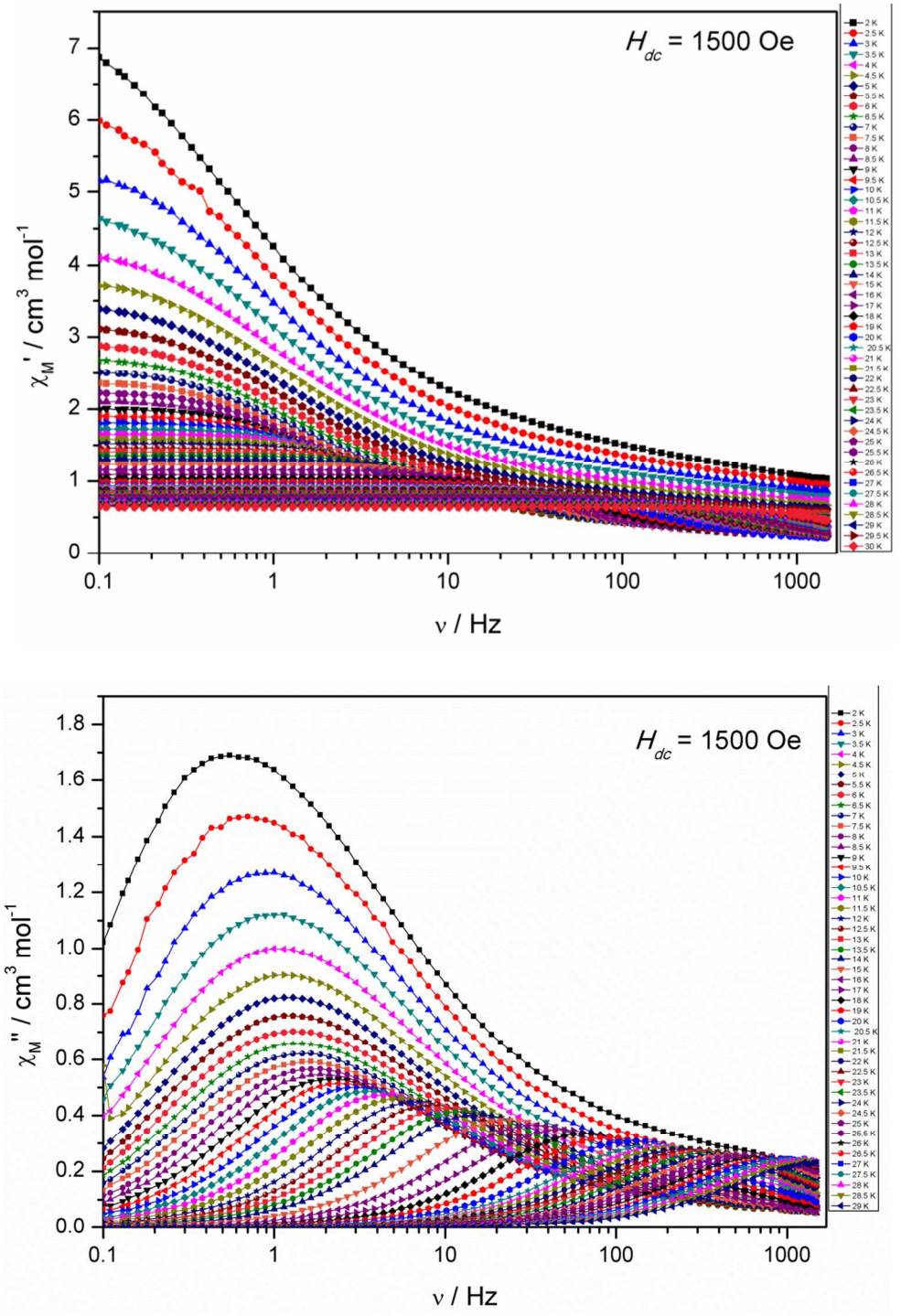

Figure S10. (top) In-phase susceptibility (χ_M') *versus* frequency for **3**; (bottom) Out-of-phase susceptibility (χ_M") *versus* frequency for **3**.

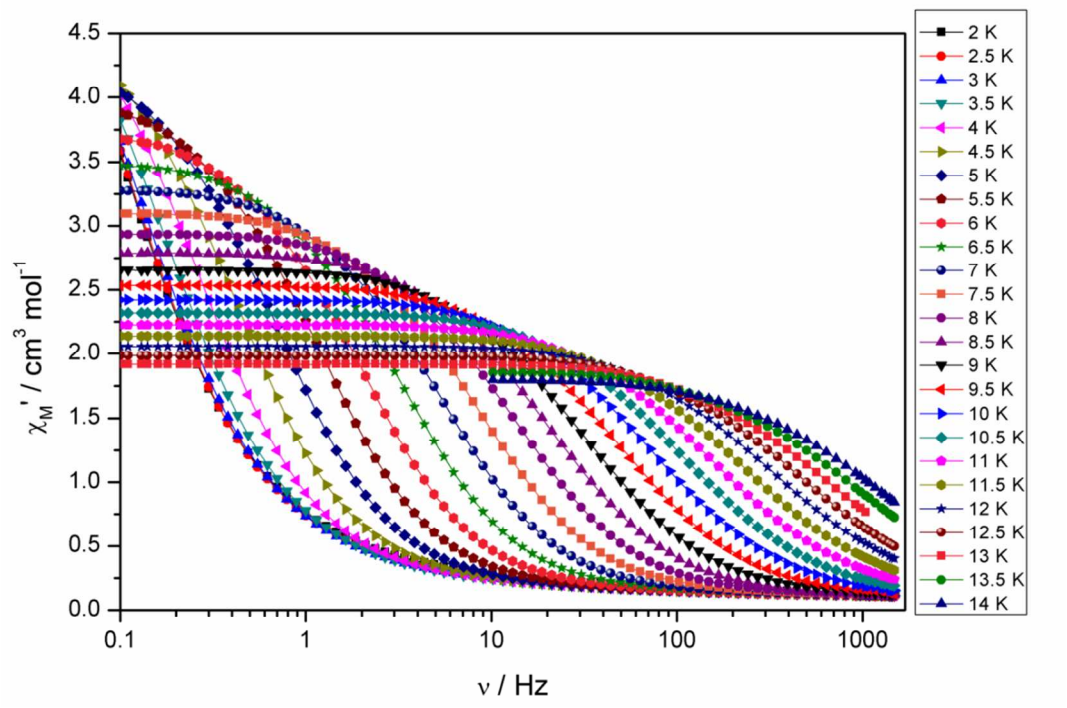

Figure S11. In-phase susceptibility (χ_M') *versus* frequency for **4**.

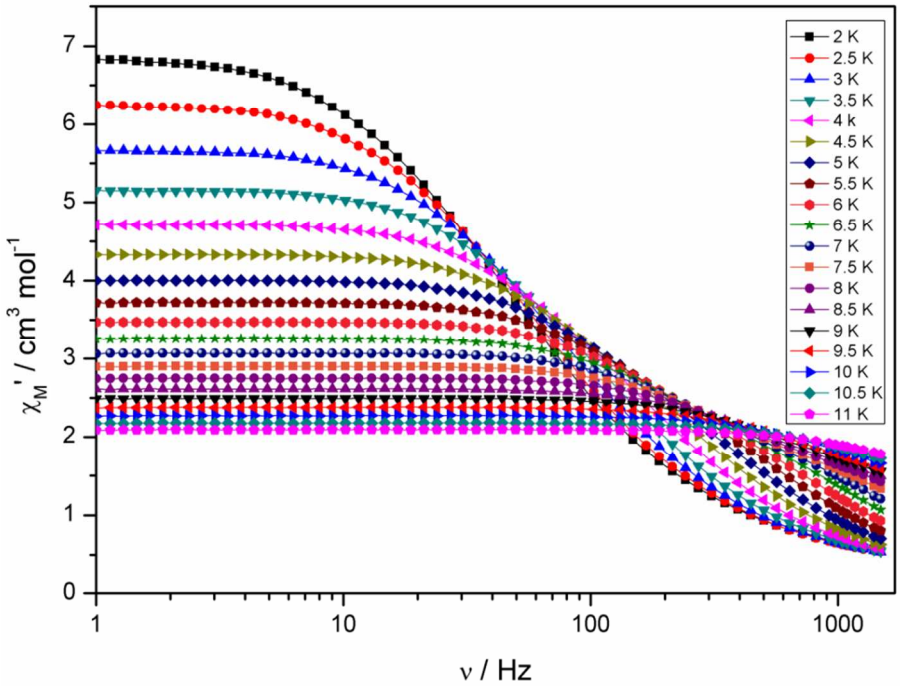

Figure S12. In-phase susceptibility (χ_M') *versus* frequency for **5**.

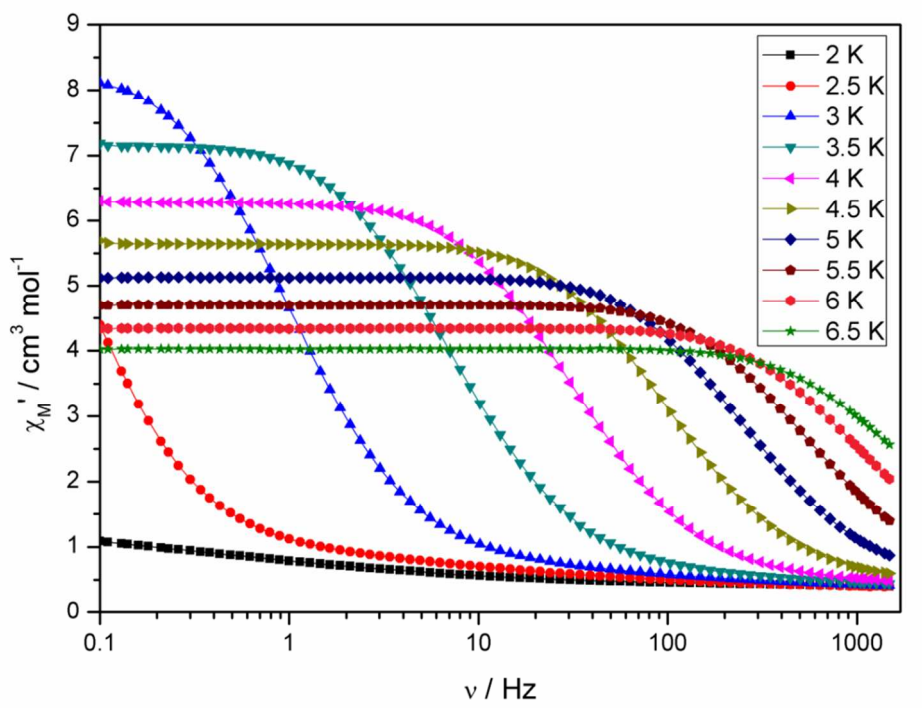

Figure S13. In-phase susceptibility (χ_M') *versus* frequency for **6**.

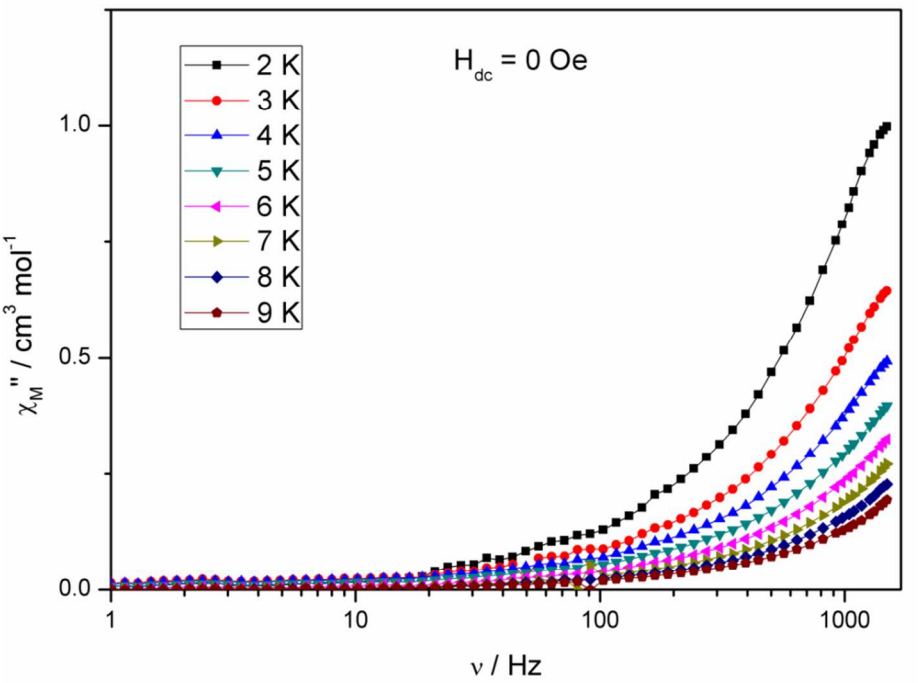

Figure S14. Out-of-phase susceptibility (χ_M") *versus* frequency for **3**, H_{ac} = 3.5 Oe and H_{dc} = 0 Oe.

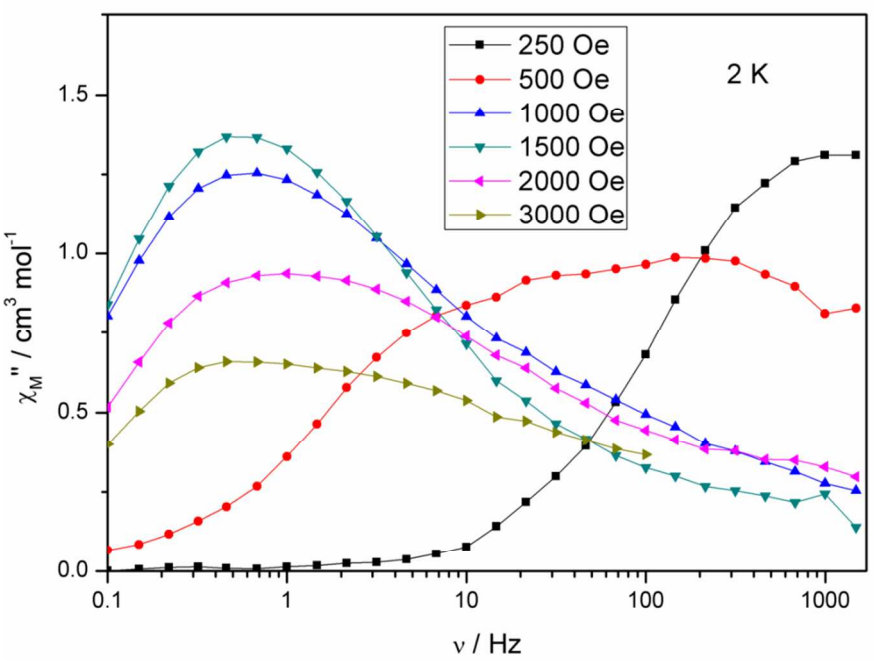

Figure S15. Isofield χ_M" *versus* frequency plot for **3**. The optimum field at which the relaxation is slowest is found to be 1500 Oe.

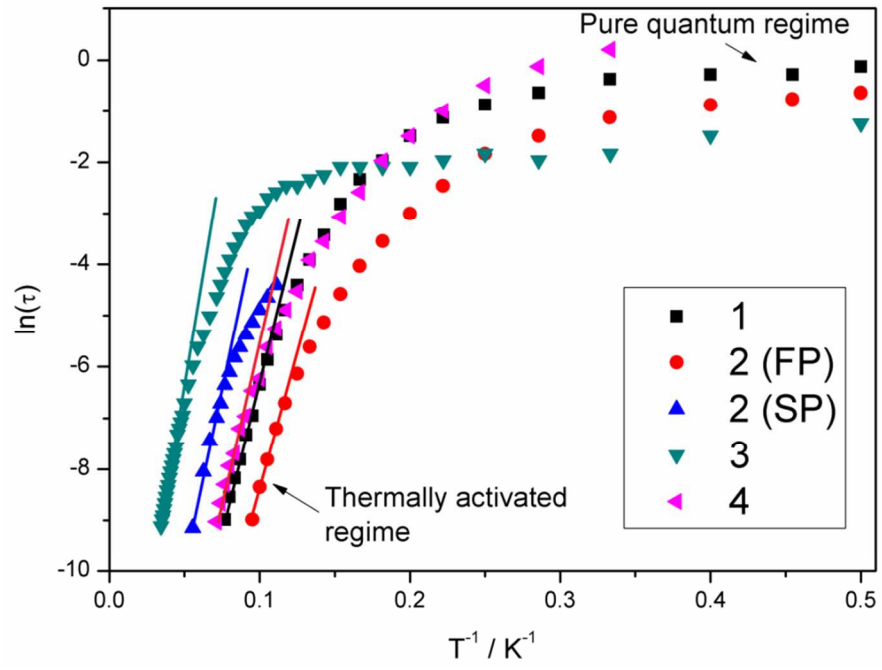

Figure S16. ln(τ) *versus* T^{-1} for **1** – **4**. The solid lines represent fits to the Arrhenius law of the thermally activated region.

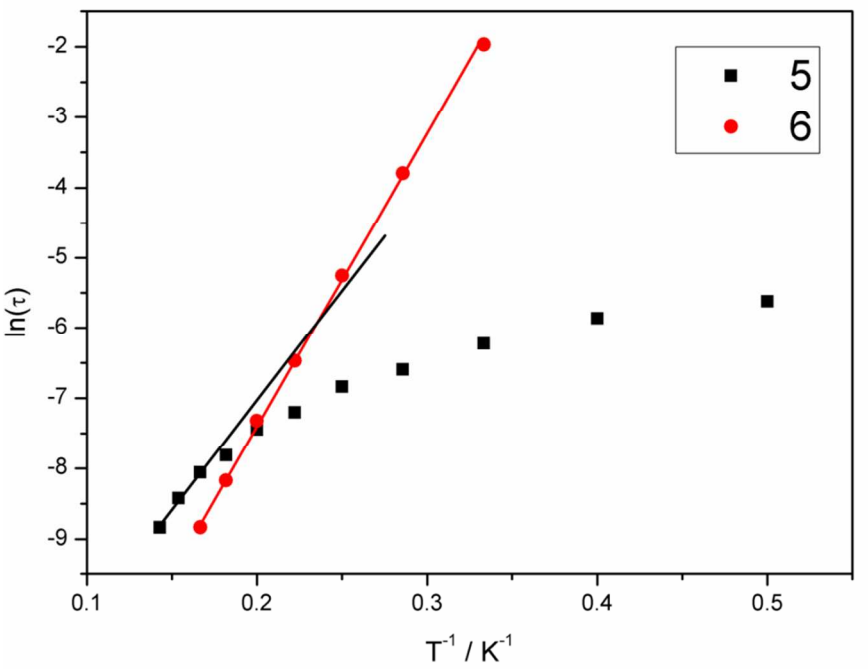

Figure S17. ln(τ) *versus* T^{-1} for **5** and **6**. The solid lines represent fits to the Arrhenius law of the thermally activated region.

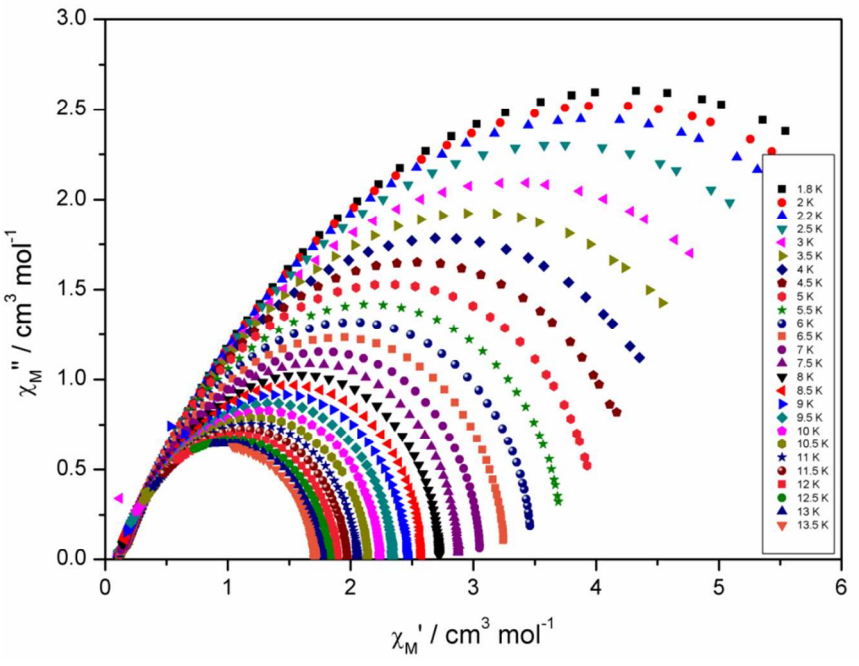

Figure S18. Cole-Cole plot for **1**.

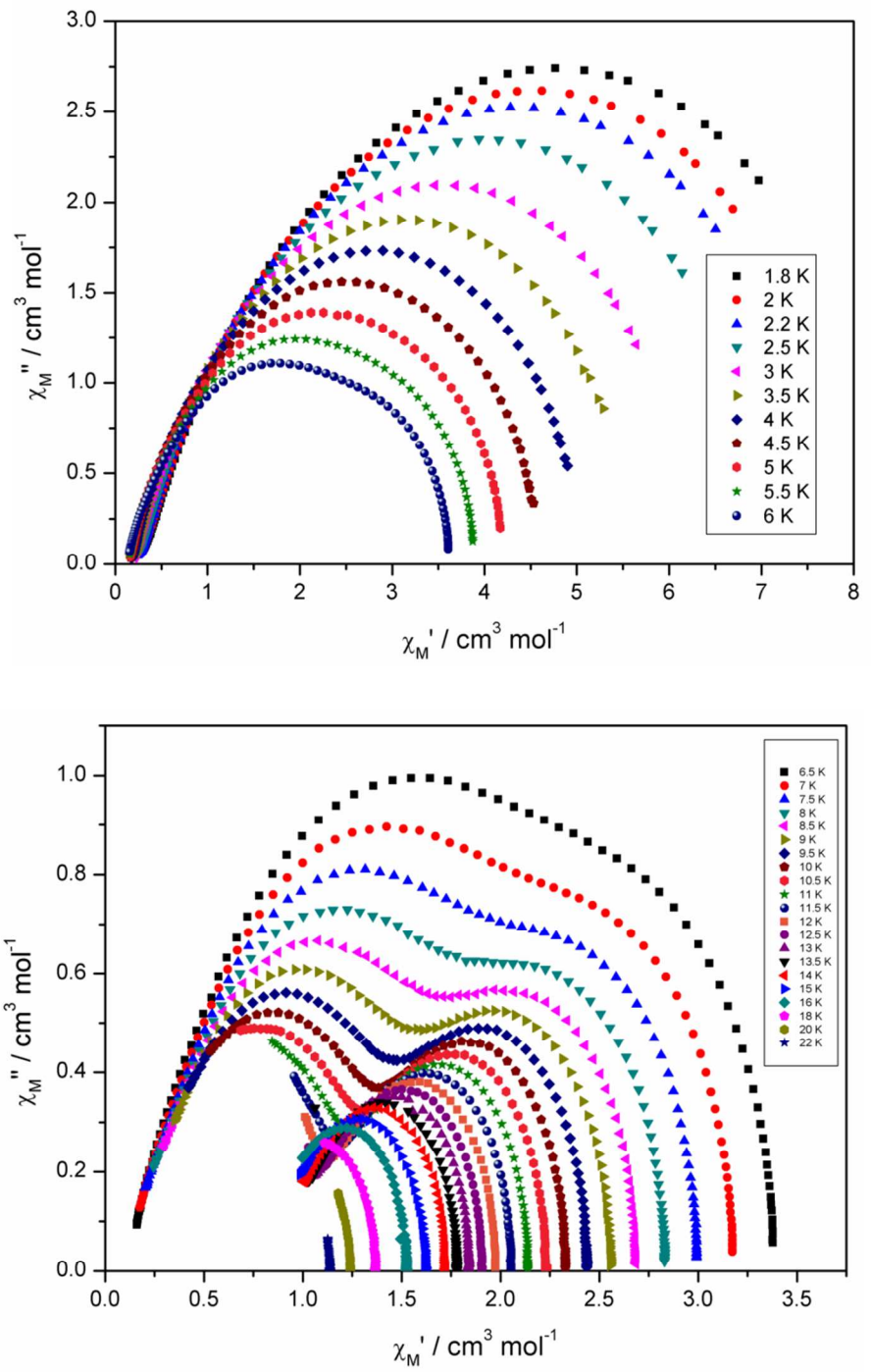

Figure S19. (top) Cole-Cole plot for **2** between 1.8 – 6 K; (bottom) Cole-Cole plot for **2** between 6.5 – 22 K, highlighting the double maxima in χ_M" and multiple relaxation processes.

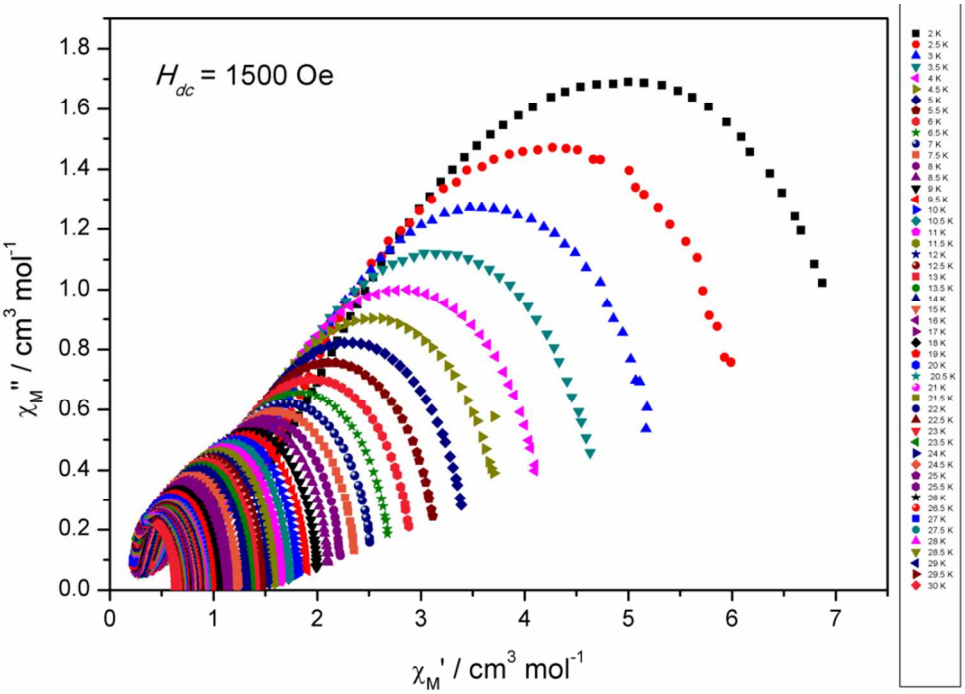

Figure S20. Cole-Cole plot for **3**.

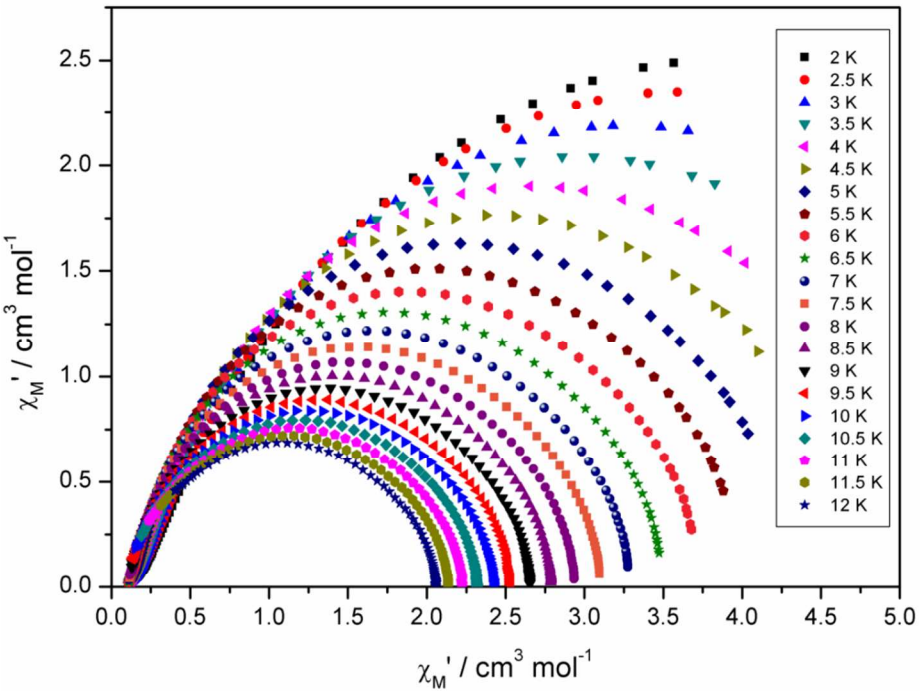

Figure S21. Cole-Cole plot for **4**.

Ab-initio Calculations

Analysis of the unsymmetrical complex 2

Computational details

All calculations were done with MOLCAS 7.8 and are of CASSCF/RASSI/SINGLE_ANISO type.

The entire molecule was computed *ab initio*.

The neighboring Dy ion was computationally substituted by diamagnetic Lu. The Co ions were kept as they are in all calculations.

Two basis set approximations have been employed: **1** – small, and **2** – large. Table 1 shows the contractions of the employed basis sets for all elements.

Table S2. Contractions of the employed basis sets in computational approximations 1 and 2.

Basis 1	Basis 2
Dy.ANO-RCC...7s6p4d3f1g.	Dy.ANO-RCC...8s7p5d4f2g1h.
Lu.ANO-RCC...7s6p4d3f1g.	Lu.ANO-RCC...7s6p4d3f1g.
Co.ANO-RCC...5s4p2d1f.	Co.ANO-RCC...5s4p2d1f.
O.ANO-RCC...3s2p1d. (close)	O.ANO-RCC...4s3p2d. (close)
O.ANO-RCC...3s2p. (distant)	O.ANO-RCC...3s2p. (distant)
N.ANO-RCC...3s2p1d. (close)	N.ANO-RCC...4s3p2d. (close)
N.ANO-RCC...3s2p. (distant)	N.ANO-RCC...3s2p. (distant)
C.ANO-RCC...3s2p.	C.ANO-RCC...3s2p.
H.ANO-RCC...2s.	H.ANO-RCC...2s.

Active space of the CASSCF method included 9 electrons in 7 orbitals (4*f* orbitals of Dy^{3+} ion).

We have mixed 21 sextets, 128 quartet and 130 doublet states by spin-orbit coupling.

On the basis of the resulting spin-orbital multiplets SINGLE_ANISO program computed local magnetic properties (g-tensors, magnetic axes, local magnetic susceptibility, etc.)

1.1 Electronic and magnetic properties of individual Dy^{III} centers

Table S3. Energies of the lowest Kramers doublets (cm^{-1}).

Dy1		Dy2	
basis1	basis2	basis1	basis2
0.000	0.000	0.000	0.000
132.493	133.214	85.407	94.547
265.747	269.182	194.142	202.895
346.886	352.538	254.337	275.976
402.643	406.330	288.209	318.999
449.642	452.814	335.621	365.787
495.897	509.949	402.075	434.321
786.585	778.730	724.540	746.382
3591.969	3591.571	3569.272	3573.686
3760.697	3759.205	3674.760	3677.817
3829.380	3831.870	3751.421	3770.180
3888.553	3895.527	3813.607	3839.241
3935.670	3946.410	3855.682	3887.701
4034.640	4033.852	3943.817	3965.821
4173.187	4167.058	4082.241	4101.342
6177.314	6175.936	6126.783	6131.313
6295.740	6295.742	6210.508	6220.503
6365.237	6368.614	6293.588	6313.868
6425.807	6435.025	6364.964	6393.380
6521.834	6519.035	6457.583	6478.440
6641.917	6637.040	6524.488	6540.458
8167.603	8166.433	8106.384	8113.392
8263.389	8263.143	8179.109	8191.975
8346.625	8354.855	8278.758	8303.350
8433.543	8430.377	8385.801	8406.254
8565.120	8560.365	8448.020	8462.478
9697.853	9696.789	9630.389	9638.955
9834.131	9837.421	9747.458	9763.757
9916.331	9916.591	9872.875	9895.487
10088.304	0082.692	9980.925	9995.288
…	…	…	…

Table S4. Energies (cm^{-1}) and *g* tensors of the lowest Kramers doublets (KD).

KD		Dy1				Dy2			
		basis1		basis2		basis1		basis2	
		E	*g*	E	*g*	E	*g*	E	*g*
1	g_X	0.000	0.005411	0.000	0.005744	0.000	0.022391	0.000	0.019676
	g_Y		0.007338		0.006981		0.028450		0.026176
	g_Z		19.840076		19.836157		19.754080		19.754644
2	g_X	132.493	0.124785	133.214	0.072098	85.407	0.215221	94.547	0.213628
	g_Y		0.181815		0.105483		0.254710		0.228804
	g_Z		17.029156		17.043070		17.024590		17.015657
3	g_X	265.747	1.965070	269.182	1.707113	194.142	0.587883	202.895	0.406913
	g_Y		2.958681		2.479018		0.792767		0.618904
	g_Z		12.944200		13.241209		14.468495		14.717421
4	g_X	346.886	3.078743	352.538	3.906455	254.337	1.160607	275.976	0.060754
	g_Y		5.325129		4.988647		2.449787		0.797216
	g_Z		9.101345		9.201199		11.884273		11.963337
5	g_X	402.643	1.786976	406.330	1.672472	288.209	9.145644	318.999	2.246455
	g_Y		3.543228		3.822062		5.811351		4.920889
	g_Z		15.934081		15.269944		0.836805		11.125568
6	g_X	449.642	0.526342	452.814	0.757069	335.621	3.777112	365.787	3.079244

	g_Y		1.064338		1.438200		5.369211	3.742817
	g_Z		14.253448		14.077146		8.141164	9.025729
7	g_X	495.897	0.221379	509.949	0.187606	402.075	0.735911	434.321	0.730951
	g_Y		0.264051		0.226526		1.857614	1.985952
	g_Z		18.834877		18.955395		15.509876	15.476005
8	g_X	786.585	0.004153	778.730	0.004722	724.540	0.005069	746.382	0.006026
	g_Y		0.006897		0.008207		0.007179	0.009338
	g_Z		19.745680		19.729317		19.644397	19.614186

Table S5. Angles between the main magnetic axes of the lowest Kramers doublet obtained in different computational approximations (degrees)

		Dy1		Dy2	
		basis1	basis2	basis1	basis2
Dy1	**B1**	0.0000	0.7238	13.3321	16.4640
	B2	0.7238	0.0000	12.6122	15.7418
Dy2	**B1**	13.3321	12.6122	0.0000	3.9599
	B2	16.4640	15.7418	3.9599	0.0000

Table S6. Angles between the main magnetic axes of the ground and first excited Kramers doublet of (degrees).

	Dy1		Dy2	
	basis1	basis2	basis1	basis2
angle	6.8852	6.5580	1.3031	4.6502

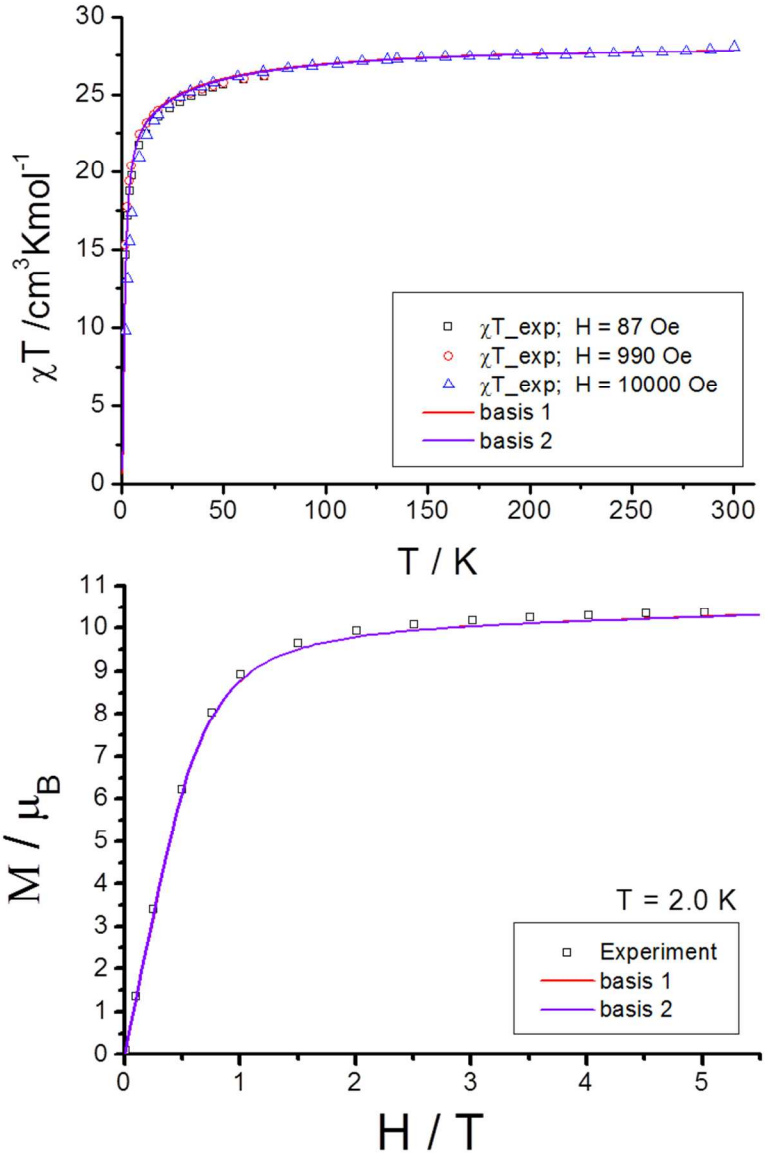

Figure S22. (top) A comparison between measured and calculated magnetic susceptibility of **2**; (bottom) Measured and calculated molar magnetization of **2** at 2.0 K.

Table S7. Energies (cm^{-1}) and the corresponding tunneling gaps and g_Z values of the lowest 4 exchange doublet states of the unsymmetrical complex **2**.

basis 1		
energy	Δ_{tun}	g_Z
0.00000000000000 0.00000045034236	4.50342E-07	4.59009
1.28990983510568 1.28991139253681	1.55743E-06	39.32538
85.49354219233560 85.49354921825949	7.02592E-06	4.76809
86.61009457441040 86.61011002740760	1.54530E-05	36.66186

basis 2		
energy	Δ_{tun}	g_Z
0.00000000000000 0.00000026564394	2.65644E-07	5.41283
1.29965701971048 1.29965840369496	1.38398E-06	39.21626
94.62728182427078 94.62728677727253	4.95300E-06	4.64139
95.76671205716472 95.76672603979175	1.39826E-05	36.66548

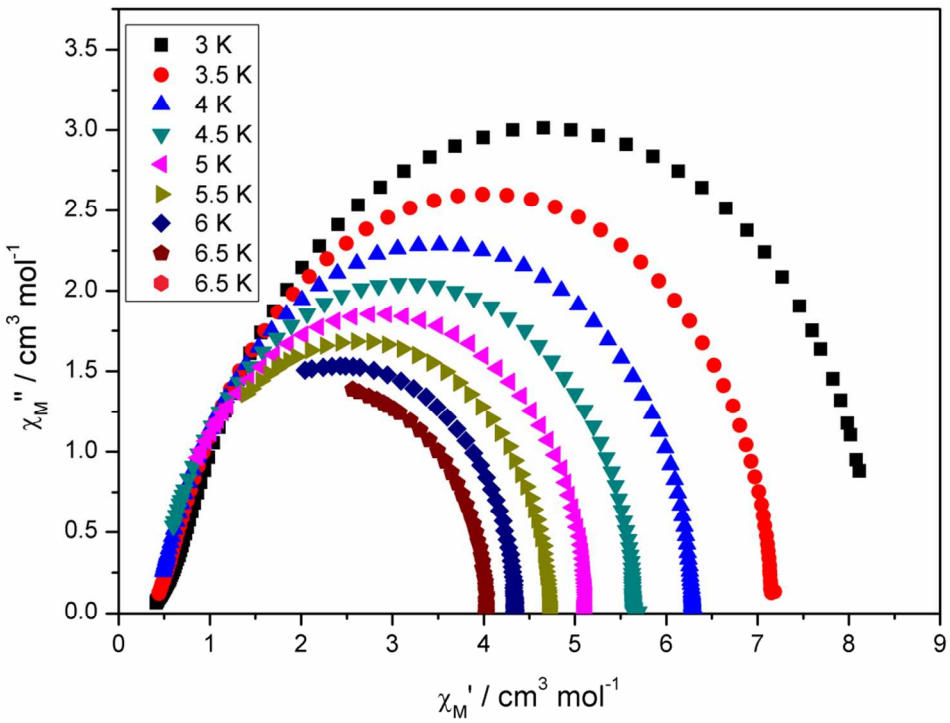

Figure S23. Cole-Cole plot for **5**.

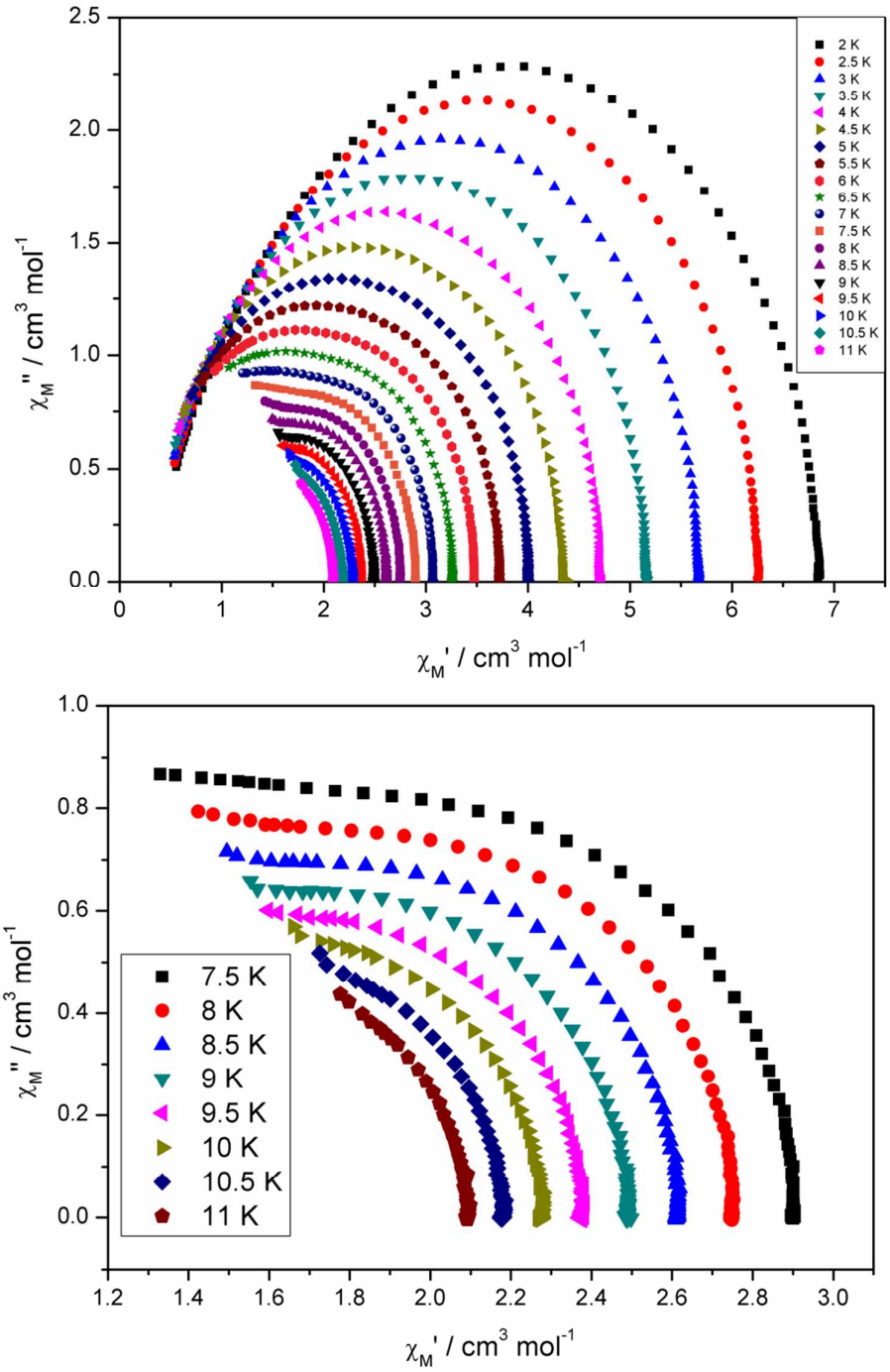

Figure S24. (top) Cole-Cole plot for **6**; (bottom) Cole-Cole plot at high temperatures exemplifying the second increase in χ_M" and the multiple relaxation mechanisms.

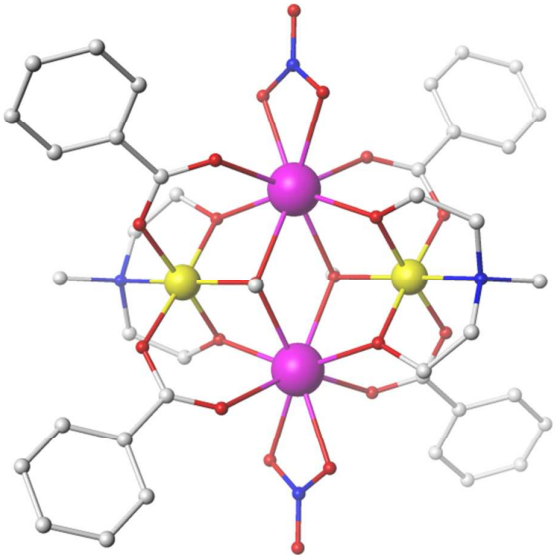

Figure S25. Molecular structure of the $[Cr^{III}_2Dy^{III}_2(OMe)_2(acac)_4(mdea)_2(NO_3)_2]$ complex. Colour scheme; Cr^{III}, yellow; Dy^{III}, purple; O, red; N, blue; C, grey